

Tension-Stabilized Coiling of Isotropic Tape Springs

Lee Wilson^{a,b}, Eleftherios E. Gdoutos^a, Sergio Pellegrino^{a,*}

^a*Graduate Aerospace Laboratories, California Institute of Technology
Pasadena, CA 91125, USA*

^b*Current address: Momentus Space, 3050 Kenneth St, Santa Clara, CA 95054, USA*

Abstract

A tape spring can be held tightly coiled on a circular cylinder by means of a tension force applied at the tip. This paper determines the smallest value of the required tension force by means of analytical methods, experiments and detailed numerical simulations. The minimum force depends on the coiling ratio, defined as the ratio between the transverse radius of the tape spring and the radius of the cylinder. It varies with an inverse quadratic relation for coiling ratios smaller than 1 (bending-dominated regime) and with a linear relation for coiling ratios greater than 3.424 (tension-dominated regime). For coiling ratios between 1 and 3.424 there is an intermediate behavior, and the required tension force is non-unique and rather small.

Keywords: packaging, deployment, large strain deployable structures, tape springs

1. Introduction

Packaging and deployment are central to the design of large spacecraft structures that have to fit in volume-constrained launch vehicles. Deployable structures are packaged and deployed through a variety of techniques, such as sliding mechanisms in telescopic booms (Arenberg et al., 2016), chemical rigidization
5 in inflatable cylindrical booms (Schenk et al., 2014), elastic deformation in coil-

*Corresponding author

Email address: sergiop@caltech.edu (Sergio Pellegrino)

URL: <http://www.pellegrino.caltech.edu/> (Sergio Pellegrino)

able masts that are stowed by deforming the longerons into intertwined helices (Mauch, 1960), and mechanical articulation in pantograph booms (Dailey et al., 1999). These well-developed deployment schemes involve complex mechanisms and often require electric motors.

A recent approach makes use of the elastic (bending) strain-energy stored during packaging to deploy composite thin shell structures. The availability of thin-ply carbon fiber-reinforced plastic (CFRP) composites has made it possible to realize deployable shell structures with areal density on the order of 100 g/m^2 . These shells can be tightly coiled, as in the family of deployable booms developed by the German Space Agency (Straubel et al., 2015, 2011). However, realizing in full the potential advantages of mechanism-free deployable structures requires a deep understanding of the coiling behavior of thin shells, which have been shown to exhibit unexpected localization, leading to complex deployment and potential damage.

For example, recent studies of Triangular Rollable and Collapsible (TRAC) booms, which consist of two tape springs bonded along a common edge, have shown that booms coiled on a cylindrical spool have a tendency to form localized folds (Leclerc et al., 2017) instead of a uniform coil, unless a small spool diameter is chosen (Murphey et al., 2017).

The present study of the coiling behavior of thin shell structures considers the prototypical strain-energy deployed structure, an isotropic, linear-elastic *tape spring*, i.e. a thin cylindrical shell with circular arc cross-section of radius R that subtends a uniform angle α , as shown in Fig. 1. The Young's modulus and Poisson's ratio of the shell are E and ν , respectively. The simplest example of this structure (where, however, close inspection will show that the cross-section is not perfectly circular) is the widely used steel tape measure.

For a simple example of localization behavior in coiled tape springs, consider a tape measure tightly coiled on a cylindrical spool, and constrained by an external cage, Fig. 2(a). As the tape spring deploys, a gap forms between the coiled tape spring and the cage, leaving the tape spring free to partially uncoil and form a series of nested localized folds, Fig. 2(b). This behavior

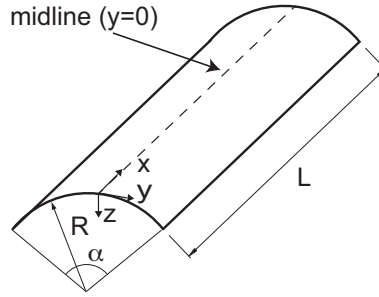


Figure 1: Geometry of tape spring and definition of key variables.

can be avoided either by applying a sufficiently large tension force at the tip of the tape spring, Fig. 2(c), or by constraining the tape spring with radial springs, Fig. 2(d). The first approach is the focus of the present paper. Both approaches have already been used in practical applications, see the tensioning mechanisms in Straubel et al. (2015) and the spring-constrained deployment mechanism in Hoskin et al. (2017). Further alternatives are to choose a spool radius that matches the natural radius of coiling of the tape spring, as explained in the next section, or to use a bistable tape spring (Pellegrino, 2005; Guest & Pellegrino, 2006), exploiting its natural tendency to remain coiled. Of these two alternatives, the first is a special case of the present study for the case of zero tension force.

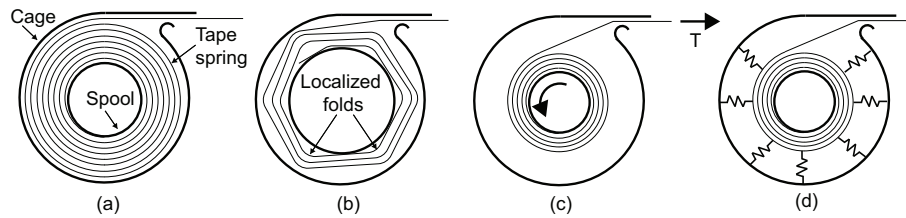


Figure 2: The tightly coiled tape spring in (a) is partially uncoiled in (b) and forms many localized folds. The folds can be avoided by applying either a tension force (c) or a series of radial spring constraints (d).

Previous work has focused on tape springs coiled around a spool with radius approximately equal to the radius R of the tape spring (Seffen & Pellegrino,

1999; Hoskin et al., 2017). The deployment of a tape spring with a single localized fold has also been studied (Seffen & Pellegrino, 1999; Mallol Parera, 2013; Stabile & Laurenzi, 2014). However, there has been no previous study that explained and/or analyzed the behavior of tape springs coiled around a
55 spool of arbitrary radius. In any case, this is what happens when coiling a long tape spring, where the effective spool radius significantly increases due to the thickness of multiple turns of tape spring. Furthermore, the effects of a tension force on the formation of localized folds in tape springs have not been studied.

To understand the range of behaviors that can be exhibited by coiled tape
60 springs, two different situations are considered in this paper. First, a tape spring that is loosely wound on a cylinder, forming several localized folds, is pulled more tightly by applying a gradually increasing tension force. For this problem, the relationship between the tension force and the extension of the tape spring is studied, as well as the sequence of shape transitions of the tape
65 spring as the number of localized folds gradually decreases. This situation is called *coiling*. Second, a tape spring is tightly wound on a cylinder, by rotating the cylinder while a large tension force is applied at the tip of the tape spring. For this problem, the value of the minimum force for which the tape spring remains uniformly coiled is determined, and the formation of localized folds
70 as the tension is further decreased is also studied. This situation, which is of greater interest for practical applications, is called *uncoiling*.

Note that coiling and uncoiling, as defined above, are different processes, and follow different equilibrium paths, resulting in macroscopically different geometric configurations of the tape spring. It will be shown, however, that the
75 two approaches lead to tension force values that are rather close.

This paper focuses on the specific case of isotropic tape springs coiled with the concave side facing out (opposite sense coiling, as explained in Section 2) and is laid out as follows. In Section 2 the basic regimes of coiling and uncoiling are defined and simple analytical models are presented. In Section 3 an experimental
80 study of the coiling process is presented. Section 4 introduces the numerical simulation techniques that were used to study coiling and uncoiling. Section 5

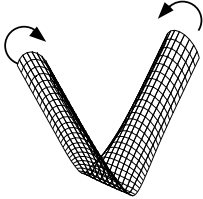
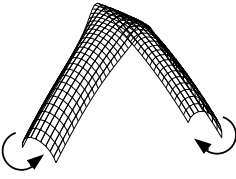
presents the simulation results. Section 6 concludes the paper. Details on the numerical studies are provided in the Appendix.

2. Uniform coiling and localized folding

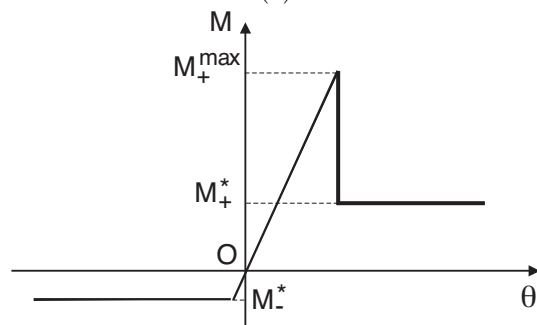
85 The basic mechanics of tape springs (Seffen & Pellegrino, 1999; Pellegrino, 2015) is briefly summarized here. A tape spring is bent in the *opposite sense* when it is loaded by a uniform bending moment $M > 0$ that applies a tensile stress along the longitudinal edges and, conversely, it is bent in the *equal sense* when the uniform bending moment $M < 0$ applies an edge stress that
90 is compressive. Tape springs bent in the two senses are shown in Fig. 3(a). For sufficiently small amplitudes of the rotation θ the tape spring is uniformly curved and its moment-rotation response is linear. For larger end rotations the tape spring snaps, suddenly in the case $M > 0$ or through a gradual process involving bending and twisting in the case $M < 0$, and the moment greatly
95 decreases. For further increases of θ , the bending moment remains constant while the arc-length of the elastic fold increases. A schematic moment-rotation relation is shown in Fig. 3(b).

On either side of the elastic fold there are transition regions that can be assumed to be invariant, joining the two transversely curved cylindrical surfaces
100 to a central, longitudinally curved surface. It has been shown (Calladine, 1988) that if the tape spring material is isotropic, the radius of curvature of the longitudinal fold is equal to the transverse radius of the tape spring. Therefore, the radius R of the tape spring is also its *natural radius of folding*. A recent study has shown that, due to the existence of boundary layers on the edges of a folded
105 tape spring, in which the tape spring retains its original transverse curvature, the natural radius of folding differs by 5 to 10% from R , and is actually different for opposite- and equal-sense bending (Calladine & Seffen, 2019).

The specific objective of the present study is the opposite sense coiling of a tape spring of radius R around a cylinder of arbitrary radius r_c , under a tension
110 T . It will be explained in the next subsections that there are three different

	Bending (small rotations)	Folding (large rotations)
Opposite sense ($M > 0$)		
Equal sense ($M < 0$)		

(a)



(b)

Figure 3: (a) Bending and folding of a tape spring (Pellegrino, 2015). (b) Schematic moment-rotation relationship.

regimes for the tape spring, each characterized by a particular type of variation for the tension T vs. the ratio r_c/R . The three regimes are defined in Fig. 4 and are characterized as follows.

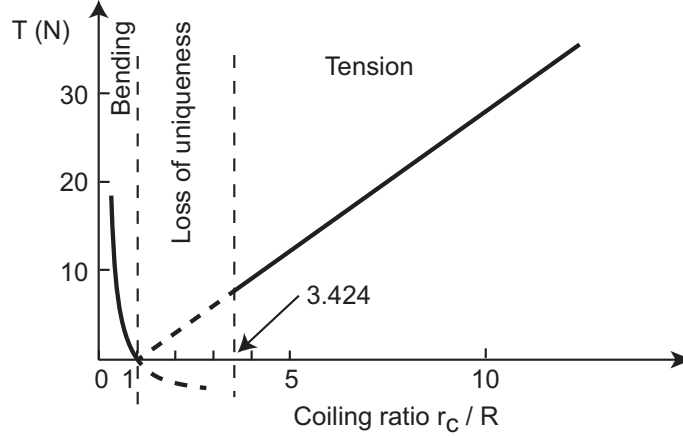


Figure 4: Three regimes of coiling of a tape spring.

- For $r_c/R \leq 1$, the behavior is *bending dominated*, resulting in a quadratic decrease of T as $r_c/R \rightarrow 1$.
- For $1 < r_c/R < 3.424$, there is a transition from bending dominated to tension dominated behavior and $T \sim 0$.
- For $r_c/R > 3.424$, the behavior is *tension dominated*, and T increases linearly with r_c/R .

The rest of this section provides a basic analysis of each regime that leads to a simple analytical model. The transitions between different regimes and the physical significance of the limits $r_c/R = 1$ and $r_c/R = 3.424$ are also explained. In the following sections, results from these simple analytical models will be compared to high fidelity numerical simulation results.

2.1. Bending-dominated regime

The bending-dominated coiling of tape springs was studied in a recent paper (Hoskin et al., 2017) and independently by one of the present authors (Wilson,

2017). Consider a tape spring with a longitudinal fold of uniform radius r that subtends an angle θ , as shown in Fig. 5. The bending strain energy in the fold is given by:

$$U(r) = \frac{D\alpha R\theta}{2} \left(\frac{r}{R^2} + \frac{2\nu}{R} + \frac{1}{r} \right) + U_{\text{transition}} \quad (1)$$

where $D = Et^3/(12(1 - \nu^2))$ is the flexural stiffness of the shell and αR is the transverse arc-length of the tape spring. $U_{\text{transition}}$ is the strain energy in the transition regions on either side of the fold.

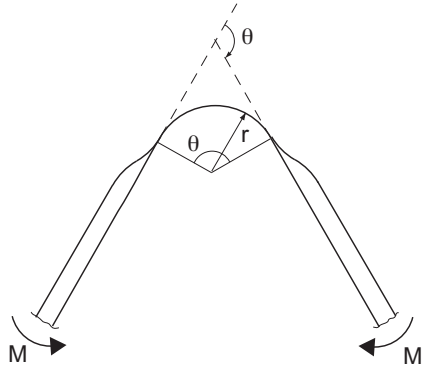


Figure 5: Tape spring with an opposite-sense fold.

It can be shown that the fold radius that minimizes $U(r)$ is $r = R$ (Calladine, 1988), and a straightforward extension to piece-wise curvilinear cross-sections of uniform thickness yields the following expression for the natural radius of folding for a tape spring whose cross-section consists of straight segments and circular arcs (an example is shown in Fig. 12(a)):

$$R = \sqrt{\frac{\sum_{k=1}^m w_k + \sum_{j=1}^n R_j \alpha_j}{\sum_{j=1}^n \frac{\alpha_j}{R_j}}} \quad (2)$$

where R_j, α_j are the radius and angle subtended by each arc and w_k is the length of each straight piece.

Next, consider a tape spring loaded by equal and opposite moments, M ,

such that

$$0 < M_+^* < M < M_+^{max}$$

In this range, two different equilibrium configurations of the tape spring are possible, either uniformly bent (actually, almost straight), or folded with a natural fold radius R .

The radius of the fold region can be changed to a general radius, r , by
 145 applying two equal and opposite axial forces T at the ends of the tape spring.
 Let the subtended angle be $\theta = 2\pi$, as shown in Fig. 6. Note that in the present
 case it is not required that the tape spring is coiled on a rigid cylinder and hence
 no cylinder is considered in the following analysis.

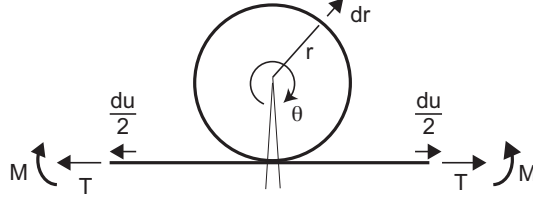


Figure 6: A single coil of a tape spring loaded by equal and opposite moments M undergoes a change of curvature in the coil due to the application of equal and opposite forces T . The positive sign convention for θ , r , u is shown.

A relationship between T and r can be obtained by considering a small
 150 configuration change, with θ constant and r varying by dr . Each end of the
 tape spring moves by $du/2$. Note the positive sign convention for T, r, u shown
 in Fig. 6.

Differentiating Eq. 1 with respect to r gives:

$$\frac{dU}{dr} = \frac{D\alpha\theta R}{2} \left(\frac{1}{R^2} - \frac{1}{r^2} \right) \quad (3)$$

where it has been assumed that $U_{\text{transition}}$ is independent of r , and hence its
 155 derivative is zero.

The change in strain energy is also equal to the work done by the tension
 force for the total extension du of the tape spring:

$$dU = T du \quad (4)$$

However, from geometry:

$$du = -\theta dr \quad (5)$$

and therefore

$$\frac{dr}{du} = -\frac{1}{\theta} \quad (6)$$

160 Combining Eqs 4, 3 and 6 yields:

$$T = \frac{dU}{du} = \frac{dU}{dr} \frac{dr}{du} = \frac{D\alpha R}{2} \left(\frac{1}{r^2} - \frac{1}{R^2} \right) \quad (7)$$

which can also be written as

$$T = \frac{D\alpha}{2R} \left(\frac{R^2}{r^2} - 1 \right) \quad (8)$$

Then, introducing inside the coiled tape spring a rigid cylinder of radius $r_c = r$, the relationship between T and R/r_c is the following inverse square law:

$$T = \frac{D\alpha}{2R} \left(\left(\frac{R}{r_c} \right)^2 - 1 \right) \quad (9)$$

165 Note that for the mode of coiling analyzed in this section no contact pressure between the tape spring and the coiling cylinder is required. Also note that the key ingredient in deriving the expression for T is the bending strain energy expression in Eq. 1. For this reason this coiling regime has been denoted as bending dominated.

170 Fig. 7 shows a plot of the axial force T to coil a tape spring in this regime. According to this figure, T rapidly approaches zero as the coiling ratio tends to 1, and becomes negative when $r/R > 1$. The value $r_c/R = 1$ corresponds to the transition from tensile to compressive forces T .

2.2. Loss of uniqueness regime

175 To form a coil with radius larger than the natural radius of folding of the tape spring, $r_c > R$, Eq. 9 requires that a compressive force is applied, which leads to the possibility that the uniformly coiled configuration of the tape spring may be unstable. An alternative is for the tape spring to become locally separated from the cylinder and in this case, when the radius of the cylinder is increased beyond

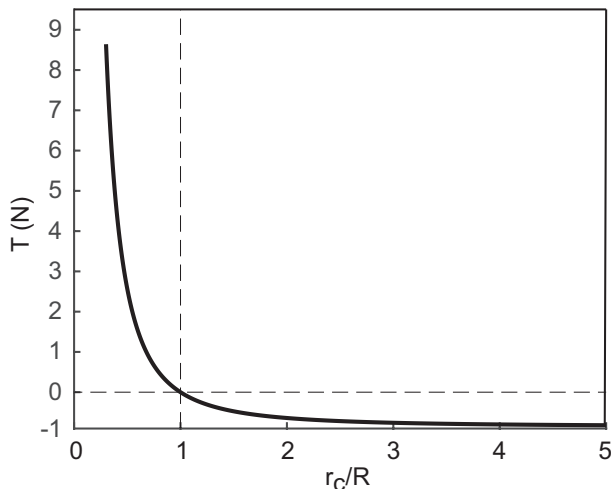


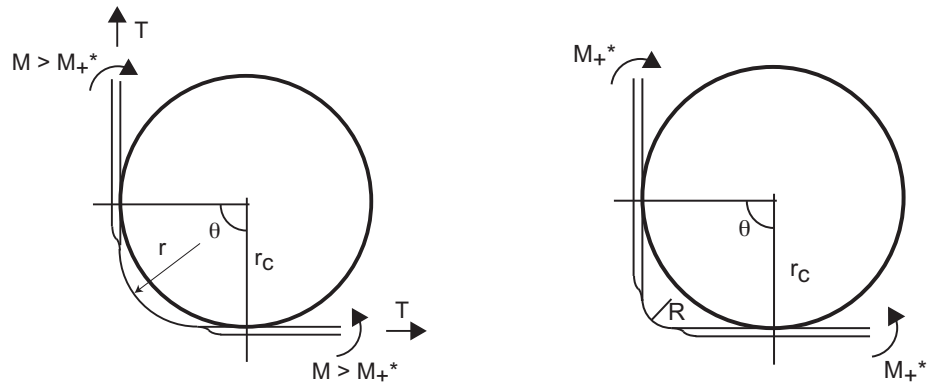
Figure 7: Variation of required tension force with coiling ratio for bending-dominated regime of tape spring with $R = 15$ mm, $\alpha = \pi/2$, $D = 0.0192$ Nm.

180 $r_c = R$, the tape spring forms an elastic fold with radius r such that $R < r < r_c$. This situations is depicted in Fig. 8(a) for a short length of tape that forms a single fold, although in a longer tape multiple folds would be formed. Note that, since $r > R$, the moment in the tape has to increase and in fact this coiling mode becomes unstable as lower-energy deformation modes exist, either with a single
 185 localized fold with the natural radius of folding, Fig. 8(b), or two folds, each with the natural radius of folding, Fig. 8(c).

The first step to compare the strain energies associated with these different configurations of the tape spring is defining the basic geometry for each case. Hence, begin by considering a tape spring with a single fold of radius R that
 190 is coiled around a cylinder of radius r_c and subtends an angle θ , as shown in Fig. 8(b). The radius mismatch results in a large gap between the cylinder and the tape spring. The length of the tape spring, see Fig. 9(a), is given by

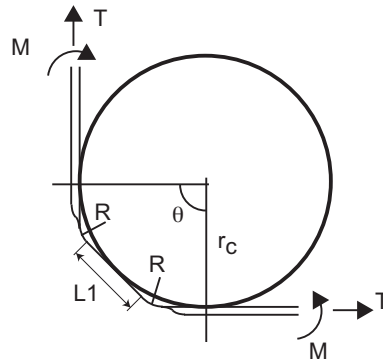
$$L = 2(r_c - R) \tan(\theta/2) + R\theta \quad (10)$$

Starting from the configuration shown in Fig. 9(a), the tape spring can be coiled a bit tighter by pulling each end by $u/2$. As u is increased, as shown



(a) One uniform fold of radius r

(b) One localized fold of radius R



(c) Two localized folds of radius R

Figure 8: Different equilibrium configurations of short length of tape spring coiled around a cylinder of radius $r_c > R$. (a) Uniform fold with general radius; (b) single fold with radius R ; (c) two localized folds with radius R . Note that the number of cylinder-to-flat transitions is two in all three configurations.

195 in Fig. 9(b), a specific value is reached for which there are two alternative configurations for the same length of tape spring. This value of u is given by:

$$u = 2 \frac{1 - \cos(\theta/2)}{1 + \cos(\theta/2)} (r_c - R) \tan(\theta/2) \quad (11)$$

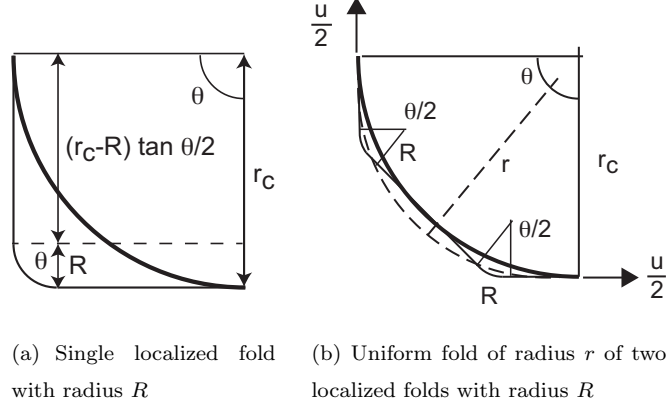


Figure 9: Three equilibrium configurations of coiled tape spring subtending an angle θ . (a) Initial configuration with natural fold radius and (b) two alternative configurations for a specific value of shortening u given by Eq. 11. Note that only the generator $y = 0$ of the tape spring is shown in the figures.

For the two configurations with a single fold the bending strain energy can be obtained from Eq. 1. For the configuration with two folds an additional term that corresponds to the length of flattened shell needs to also be included and, after the substitution $r = R$, the strain energy expression can be simplified to

$$U = D\alpha\theta(1 + \nu) + \frac{D\alpha}{2} \frac{L_1}{R} + U_{\text{transition}} \quad (12)$$

where L_1 is defined in Fig. 8(c) and has the expression

$$L_1 = u \frac{\cos(\theta/2)}{1 - \cos(\theta/2)} \quad (13)$$

and $U_{\text{transition}}$ is unchanged from the previous case as the number of transition regions is still two. Note that in Fig. 8(c) the tape spring is transversely flat between the two folds.

205 A comparison of the strain energies for these three different configurations, as a function of r_c/R , is shown in Fig. 10 for $\theta = \frac{\pi}{2}$. The cases of one fold

(corresponding to the curve labelled U_1), two folds (curve labelled U_2), and uniform radius r_c (curve labelled U_c) have been plotted. The plots of U_2 and U_c are for tape springs of equal length $L - u$, where L and u are given by Eqs 10-11.

210 This plot shows that the configuration with radius r_c (curve labelled U_c) has a higher strain energy than both other cases. It also shows that the two-fold configuration (curve labelled U_2) becomes the lowest energy configuration beyond $r_c/R > 3.424$. Based on this result, it is concluded that $r_c/R = 3.424$ is the limit for single-fold configurations of a tape spring. In fact, it has been
 215 found that around this value of r_c/R a different type of behavior, described in the next section, takes over.

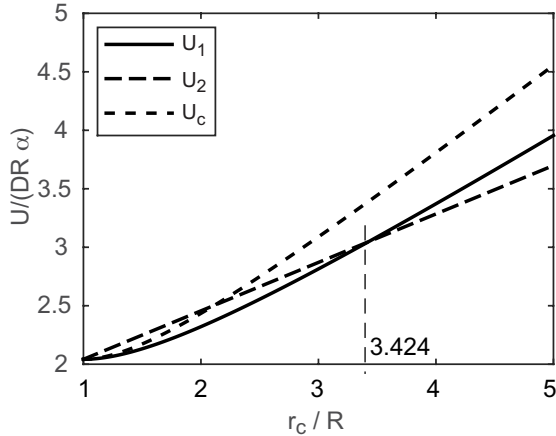


Figure 10: Comparison of bending strain energies for one-fold, U_1 , two-fold, U_2 , and uniformly coiled, U_c , tape spring configurations. The plots shown are all for $\theta = \pi/2$.

2.3. Tension-dominated regime

The third regime occurs for cylinders with radii $r_c > 3.424R$. This regime can be understood by considering a tape spring of fixed transverse radius R ,
 220 which is coiled on cylinders of increasingly larger radii. Coiling requires the *transverse flattening of the tape spring*, by a fixed amount corresponding to the curvature change $1/R$, followed by a *decreasing amount of longitudinal bending of the flattened tape spring*. Since the tension-dominated regime begins for

$r_c/R > 3.424$, it is reasonable to assume $r_c \gg R$ and therefore, the longitudinal
 225 bending moment in the flattened tape spring tends to become negligibly small
 in comparison with the transverse bending moment. Instead of being bent
 longitudinally by end moments, the tape spring deforms under the action of a
 transverse pressure. This pressure against the cylinder is the result of the axial
 tension T together with the longitudinal curvature of the tape spring, as shown
 230 schematically in Fig. 11.

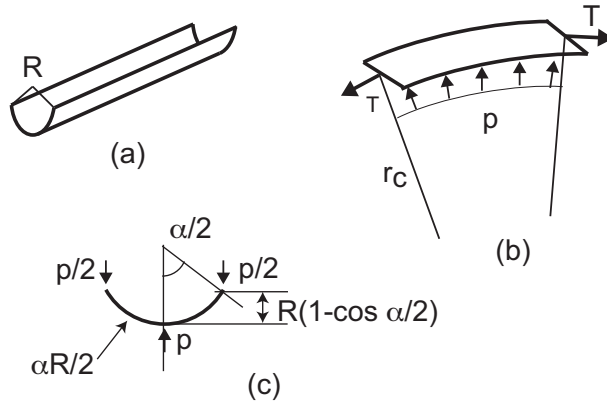


Figure 11: Transverse flattening and longitudinal bending of a tape spring with $r_c \gg R$. (a) Unstressed configuration; (b) flattened and longitudinally bent configuration; (c) transverse loads on a section of tape spring.

Equilibrium of the transversely flattened and longitudinally coiled tape spring
 in Fig. 11(b) requires:

$$T = pr_c \quad (14)$$

where p is the pressure per unit length of tape spring.

A simple estimate of the value of p can be obtained by setting the tip deflection
 235 of a cantilever with length $\alpha R/2$ and loaded by a tip force of $p/2$, equal
 to the edge height of the cross-section of the tape spring:

$$\frac{(p/2)(\alpha R/2)^3}{3D} = R - R \cos(\alpha/2) \quad (15)$$

Substituting $p = T/r_c$ from Eq. 14 and solving for T gives:

$$T = \frac{48D(1 - \cos(\alpha/2))}{\alpha^3 R} \frac{r_c}{R} \quad (16)$$

In conclusion, for a tape spring of given R in the tension-dominated regime T is proportional to r_c/R , as anticipated in Fig. 4.

240 **3. Experimental study of coiling**

This section presents a coiling experiment to obtain a reference result for the numerical solutions presented in the following sections. The tension needed to coil a commercial steel tape measure was measured for the specific case of tension-dominated behavior.

245 *3.1. Experimental setup*

The tape spring tested was a 1 inch wide Contractor Grade steel tape measure by Sears Roebuck and Co. The tape’s Young’s modulus was $E = 210$ GPa and the Poisson’s ratio $\nu = 0.3$. The cross section was piece-wise curvilinear, as shown in Fig. 12(a), and the geometric parameters are provided in
250 Table 1.

Table 1: Geometry of tested tape spring

R_1	19.2 mm
R_2	12.2 mm
w_1	3 mm
α_1	23.2°
α_2	9.5°

The natural radius of folding of this tape spring, computed from Eq. 2, is $R = 19.2$ mm.

The experimental setup is shown in Fig. 12(b). The tape spring was bent around a steel cylinder (paint can) of radius $r_c = 82.5$ mm, corresponding to a
255 coiling ratio $r_c/R = 4.3$. The cylinder was attached to the base of an Instron materials testing machine through a mounting plate. One end of the tape spring was attached to the cylinder, then the tape spring was folded around the cylinder

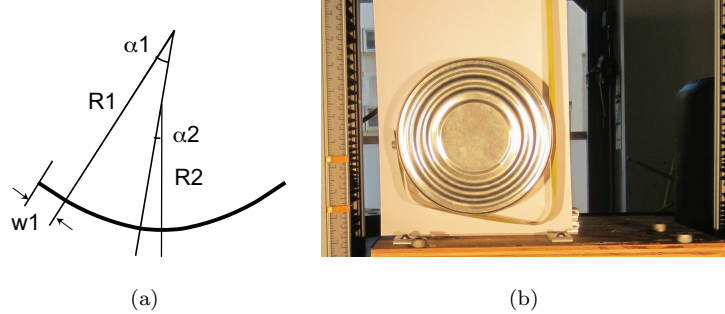


Figure 12: (a) Piecewise curvilinear cross-section of tape spring used in experiment; (b) setup for wrapping a tape spring around a cylinder of radius $r_c = 4.3R$.

by creating two localized folds and finally the non-clamped end was attached to the load cell of the testing machine. The coiling experiment consisted in moving
 260 the cross beam of the machine at a uniform rate (22 mm/min) while measuring the force applied to the tape spring. The experiment was repeated three times and the force profiles measured by the Instron load cell were averaged.

The kinetic friction coefficient between the tape spring and the cylinder was measured using a 3 mm wide by 500 mm long strip cut from an actual tape
 265 spring. The strip was wrapped once around the cylinder, and a mass of 0.250 kg was hung at the end. The other end of the strip was attached to the load cell of the testing machine and was pulled by moving the cross beam at a rate of 22 mm/min. The test was repeated nine times using the same strip.

The mean force F measured in this test was used to calculate the coefficient
 270 of friction using the capstan equation (Prentis, 1979):

$$F = T_0 e^{\mu\gamma} \quad (17)$$

where T_0 is the force applied by the hanging mass. From Eq. 17:

$$\mu = \frac{1}{\gamma} \ln \left(\frac{F}{T_0} \right) \quad (18)$$

where $T_0 = 2.45$ N, and $\gamma = 2\pi$ rad is the total angle subtended by the strip around the cylinder. The measured friction coefficient was $\mu = 0.18 \pm 0.012$.

3.2. Experimental results

275 The average force measurement profile from three experiments is shown in Fig. 13 and key snapshots from the experiments are shown at the bottom of the figure. Note that the pulling force was nearly zero until the straight section between the two localized folds came into contact with the cylinder (photo labeled a) and then the left localized fold began to increase in radius. This behavior corresponded to a smooth increase in force between the points labeled 280 (a) and (b). At an extension of 26.7 mm the force reached a maximum of 2.4 N, before beginning to decrease. At an extension of 29.5 mm the left localized fold bifurcated into two, see the photo labeled (c), as the force suddenly dropped to 0.18 N. The process of smooth increases in force, corresponding to a localized 285 fold increasing in radius, followed by sharp drops in force corresponding to a fold bifurcation, repeated as four, five, and six localized folds formed in the tape spring, at extensions of 50.5, 56.5 and 59.2 mm, see the photos labeled (d, e, f). Once six localized folds had formed the folds began to increase in radius until the whole tape spring conformed to the cylinder surface.

290 4. Numerical simulation strategies

Due to the unstable force-extension behavior observed in the experiment described in Section 3, the coiling and uncoiling behaviors are expected to be different. To understand and quantify the differences, both coiling and uncoiling of a particular tape spring on cylinders of different radii, including the configuration 295 tested experimentally in Section 3, were simulated with the commercial finite element software LS-Dyna. All solutions were computed using the explicit solver in LS-Dyna; further details on the analysis are provided below.

All simulations used the same tape spring properties ($\nu = 0.3$, $E = 210$ GPa, $\rho = 8050$ kg/m³, and $R = 19.2$ mm, as in the experiment), varying the 300 cylinder radius from $r_c = 10$ mm to 400 mm to explore the tape spring behavior for a range of coiling ratios. The length of the tape spring in each finite element model was chosen such that the free length, i.e. the length of tape spring between

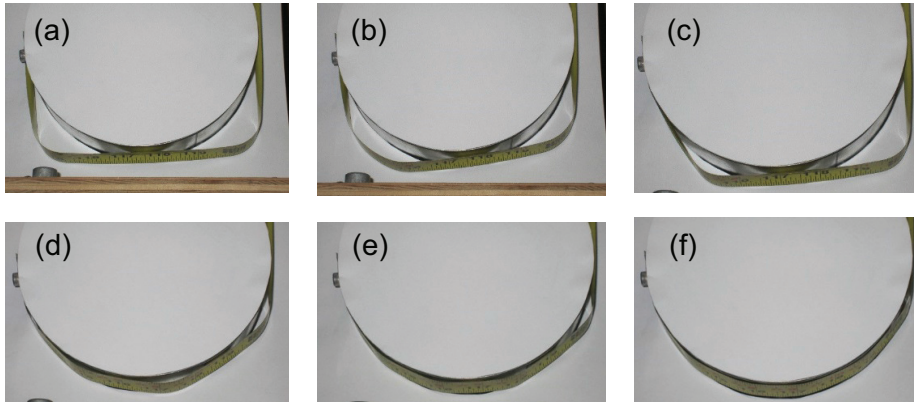
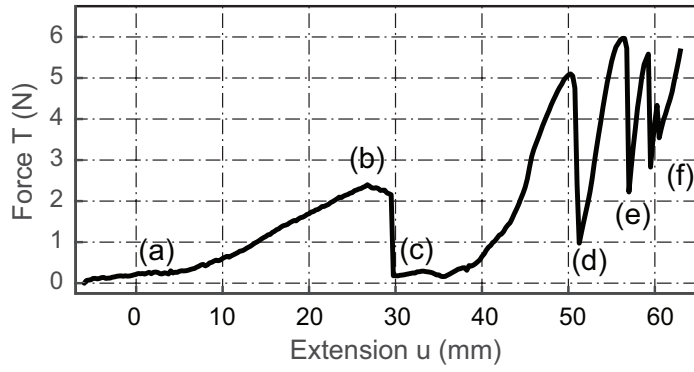


Figure 13: Force profile (average of three repeated experiments) corresponding to the wrapping of a steel tape spring around a steel cylinder along with snapshots of key stages in the experiments, labeled (a)-(f). In these experiments $r_c = 4.3R$.

the cylinder and the point where the force was applied, exceeded the transition length. This length was defined as the distance between two spikes in the plot
 305 of the bending energy per unit length of tape spring.

4.1. Coiling simulation setup

The finite element model of the initial configuration is shown in Fig. 14(a). Simulations for geometries with $r_c/R > 3$ involve longer tape springs and in this case one of end of the tape spring can be clamped, as shown in Fig. 14(b).
 310 This boundary condition closely matches the boundary condition of the experiment presented in Section 3. On the other hand, simulations for geometries with $r_c/R < 3$ involve shorter tape springs and in this case the clamped boundary condition had to be replaced with a pinned end condition at a distance $L_A = 100$ mm, to avoid an artificial increase of the force magnitude. The
 315 corresponding folded configuration is shown in Fig. 14(c).

The tape spring was meshed with 2 mm C^0 triangular shell elements.¹ The temporary cylinders and the coiling cylinder were modeled as rigid bodies, fully constrained in all degrees of freedom. Frictional contact between the coiling cylinder and the tape spring was modeled with the experimentally determined
 320 friction coefficient $\mu = 0.18$. Contact damping of $\xi = 5\%$, acting perpendicular to the contact surfaces was applied to reduce the noise in the force output due to vibration. LS-Dyna calculates the critical damping as $\xi = 2m\omega$ where m is the minimum of the master (m_{master}) and slave (m_{slave}) node masses during contact, and $\omega = \sqrt{k \frac{m_{slave} + m_{master}}{m_{slave} m_{master}}}$, where k is the interface stiffness (Hallquist,
 325 2007).

The simulations started with the tape spring in the fully deployed configuration, as shown in Fig. 14(a). To fold the tape spring into the initial two-fold configuration, Figs 14(b-c), temporary boundary conditions were applied by means of four temporary cylinders of radius 20 mm to flatten the tape spring at
 330 the two fold locations. After flattening, these temporary boundary conditions

¹Results of a mesh convergence study are presented in the Appendix.

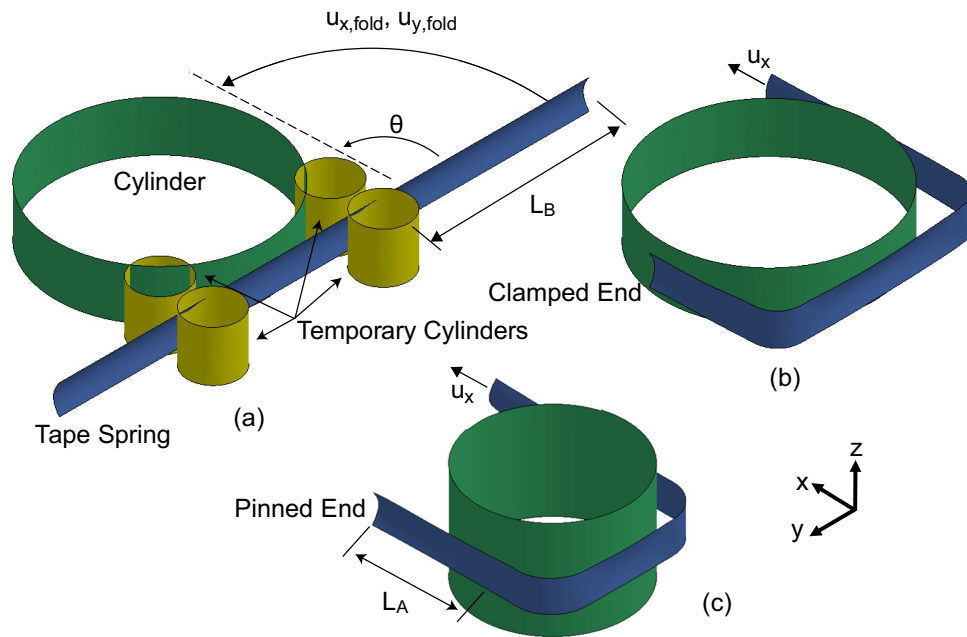


Figure 14: (a) Initial configuration of coiling numerical simulation. Two localized folds are introduced by imposing the displacements $u_{x,fold}, u_{y,fold}$ as shown and the temporary cylinders are then removed. The results are shown in (b) for $r_c/R > 3$ and (c) for $r_c/R < 3$. During the following part of the simulation, the displacement u_x shown is applied to coil the tape spring.

were removed and frictionless contact with the four cylinders was enabled².

The displacement boundary conditions $u_{x, fold}$ and $u_{y, fold}$ were imposed to coil the tape spring through an angle θ :

$$\begin{aligned} u_{x, fold} &= r_s(1 - \cos \theta) + (L_B - r_s \theta) \sin \theta \\ u_{y, fold} &= r_s \sin \theta + (L_B - r_s \theta) \cos \theta - L_B \end{aligned} \tag{19}$$

Contact with the temporary cylinders was then removed and the tape spring
 335 was allowed to find an equilibrium configuration. Mass nodal damping was applied to remove any excess kinetic energy. This simulation technique resulted in a two-fold configuration, as shown in Fig. 14(b-c). Details of the applied boundary conditions, contact conditions, and corresponding node sets are given in Table 3 and Fig. 23 in the Appendix.

340 As the extension u_x of the tape spring was increased, it was critical to determine at which stage of the simulation the tape spring would be considered to be fully coiled. The fully coiled configuration was defined such that the centerline of the tape spring conformed to the cylinder surface to within three tape spring thicknesses over a region defined by $\gamma_{min} \leq \gamma \leq \gamma_{max}$. The range
 345 $\gamma_{min}, \gamma_{max}$ was chosen to remove localized effects near the the clamped end and the first point of contact between the tape spring and the cylinder.

4.2. Uncoiling simulation setup

To investigate the uncoiling behavior, a finite element model was developed in which the tape spring was fully coiled under a sufficiently large tension force,
 350 and the magnitude of the force was then slowly decreased until a small separation between the tape spring and the cylinder had developed. This condition defined the minimum force required to keep the tape spring fully coiled.

The simulation setup is shown in Fig. 15. The simulation started with the tape spring in the fully deployed configuration, Fig. 15(a). To fold the tape
 355 spring into an initial single-fold configuration, boundary conditions were applied

²LS-Dyna keyword: automatic surface to surface.

to the tape spring edges to flatten it near the intended location of the fold. These boundary conditions were then removed and contact with the two temporary cylinders and with the coiling cylinder was enabled. The temporary cylinders force the tape spring to remain flattened. Displacement boundary conditions were then applied to the left end of the tape spring, completely constraining the motion of this end of the tape spring to the temporary cylinder.

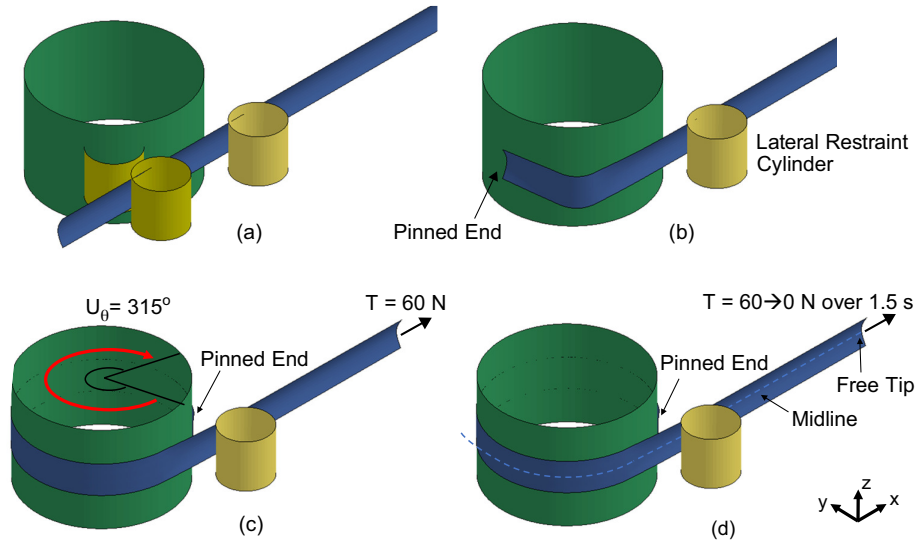


Figure 15: Uncoiling simulation setup. (a) Initial configuration, (b) single-fold configuration, (c) tension force applied to the tape spring tip, and cylinder and pinned end rotated through angle u_θ , and (d) configuration at start of unloading step.

Contact with the temporary cylinders was then removed and the tape spring was allowed to find an equilibrium configuration. Numerical damping was applied to remove excess kinetic energy. This resulted in the single-fold configuration shown in Fig. 15(b). A tension force of $T = 60$ N was then applied at the end of the tape spring, tightly coiling the tape spring through an arc of about 90° . Finally, a rotational boundary condition $u_\theta = 315^\circ$ was imposed on the cylinder with the end of the tape-spring pinned to it, to obtain the coiled configuration of Fig. 15(c).

The tension force was then reduced from 60 N to 0 N linearly over a period

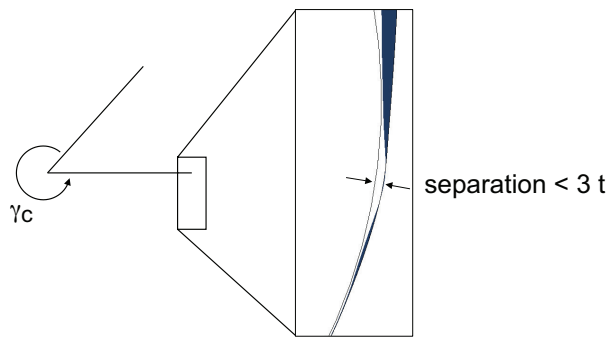
of 1.5 s and the simulation was monitored to identify the formation of localized folds. Two different methods were used to identify the formation of localized folds and hence determine the point at which the tape spring ceased to be fully conformed to the cylinder: (a) when the distance of the tape spring midline
 375 from the cylinder exceeded 3 times the thickness of the tape spring over the region in which the first localized fold forms, i.e. for angles $305^\circ < \gamma_c < 315^\circ$, Fig. 16(a); (b) when the first spike in the derivative of the tip deflection with respect to the force was observed, Fig. 16(b).

5. Simulation results

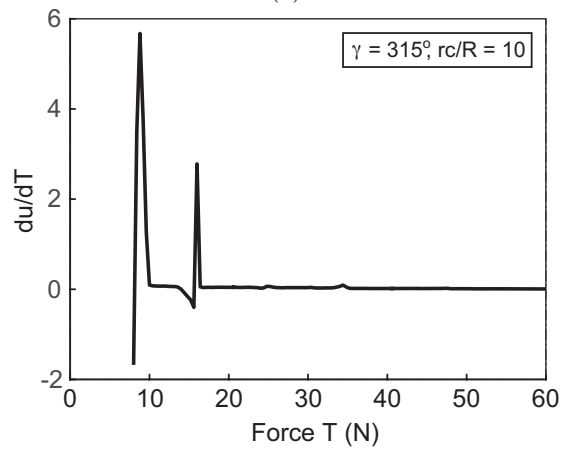
380 Results from the coiling and uncoiling simulations are presented in this section. Each type of simulation begins with a preliminary phase during which the tape spring reaches an initial configuration that either has two folds as detailed in Section 4.1, or is smoothly coiled as in the case presented in Section 4.2. The particular simulation that was compared with the experiments had a non-
 385 zero friction coefficient ($\mu = 0.18$), whereas all other simulations had $\mu = 0$ for generality.

5.1. Coiling

A simulation for the case $r_c/R = 4.3$ and $\mu = 0.18$ was performed to model the experiment presented in Section 3. The initial folded configuration is shown
 390 in Fig. 17(a). As the tip extension u_x was increased in the simulation, the localized folds bifurcated, with the progression shown in Fig. 17. In the initial configuration, at $u_x = 0$, the folds radius is 19 - 20 mm, in agreement with the theoretically predicted natural radius of folding, $R = 19.2$ mm. As u_x was increased, the localized fold closest to the clamped end increased in radius. At
 395 $u_x = 27.3$ mm the fold changed from a constant radius to one having two regions of high curvature at each end of the fold, joined by a flattened, almost straight section in between. At $u_x = 27.5$ mm the fold bifurcated into two distinct folds of radius $\approx R$. At $u_x = 62.6$ mm, see snapshot (f), three of the six localized folds fully conformed to the cylinder.



(a)



(b)

Figure 16: Two methods to determine whether the tape spring is fully conformed to the cylinder. (a) Separation between midline of tape spring and cylinder greater than 3 times the tape spring thickness over a range of angles γ_c ; (b) spike in derivative of tape spring tip displacement with respect to force.

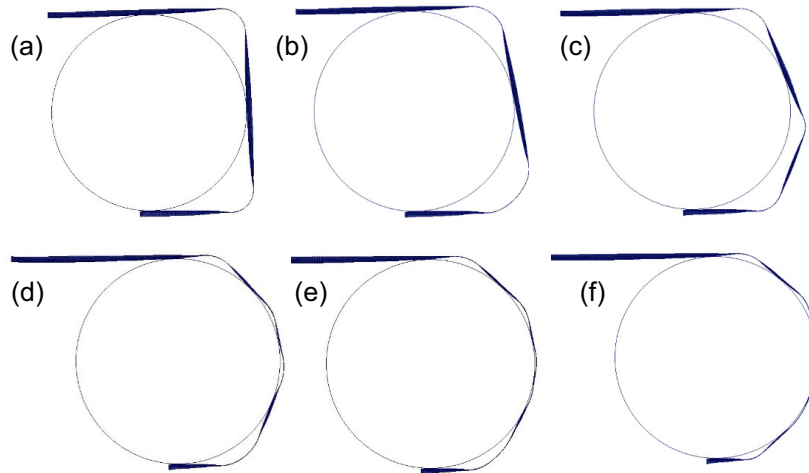
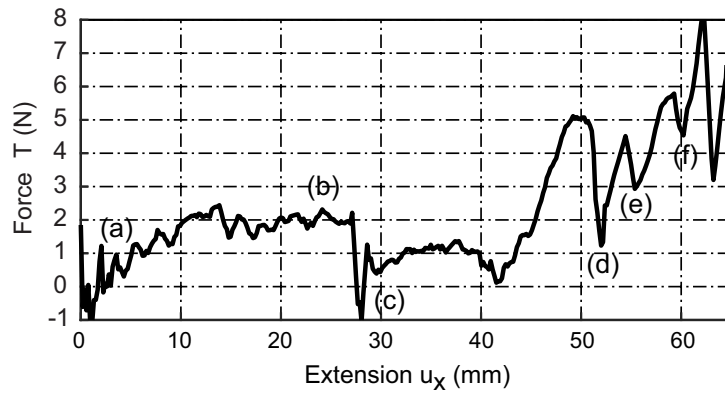


Figure 17: Force vs. extension plot obtained from coiling simulation for $r_c/R = 4.3$ along with snapshots from simulation at points (a)-(f).

400 A total of 20 simulations were carried out for the same tape spring and cylinders of different radii, with coiling ratios in the range $0.4 < r_c/R < 5.25$. The minimum tension force required to achieve full coiling has been plotted in Fig. 18. Note the similarity of this figure with Fig. 4, where the three regimes of coiling were first introduced.

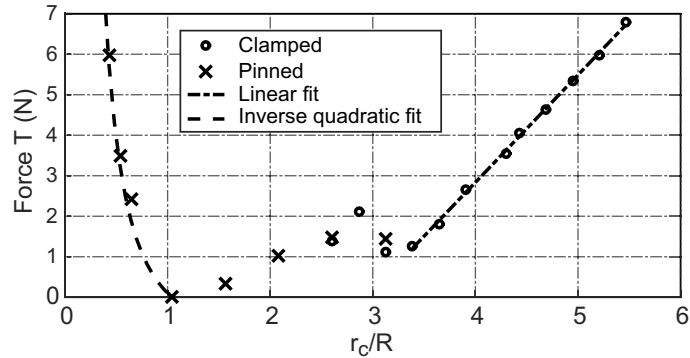


Figure 18: Minimum tension force required for a tape spring to fully conform to a coiling cylinder. The boundary conditions were clamped and pinned, respectively, for data points marked with circles and crosses.

405 5.2. Uncoiling

The force profile for an uncoiling simulation with $r_c/R = 4.3$ is shown in Fig. 19. As the tension force was decreased, a single localized fold first appeared at 3.8 N, as shown in snapshot (a). As the force continued to decrease the tape spring separated further from the cylinder in the region of this fold. Once the fold had sufficiently developed, a second localized fold developed further along the tape spring at a force of 2.4 N, as shown in snapshot (b). This process continued, with additional folds forming at 1.1 N and below, until seven localized folds spanned the entire length of the tape spring at a force of 0.53 N. As the force was decreased further the radius of curvature of the folds started to increase and the localized folds started to merge to six folds at 0.40 N, snapshot (e), and then to five folds at 0.13 N, snapshot (f).

Note that the final configuration, corresponding to $F = 0$, does not match

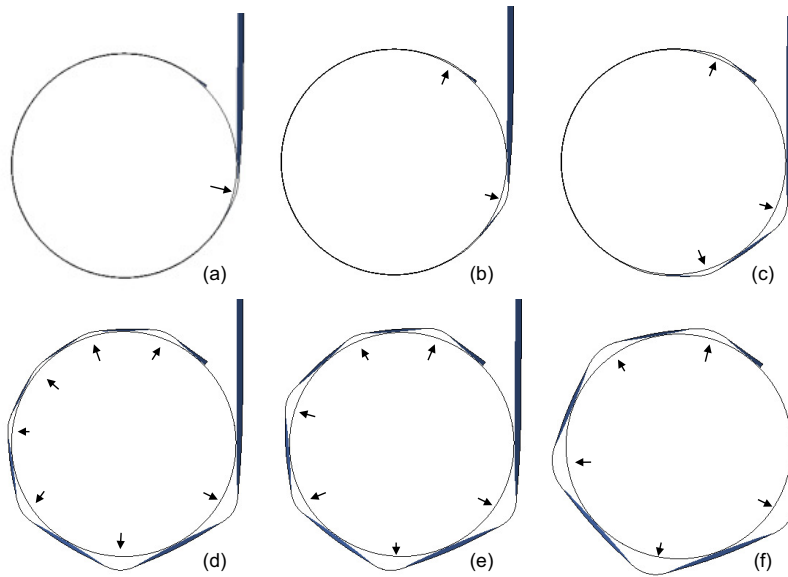
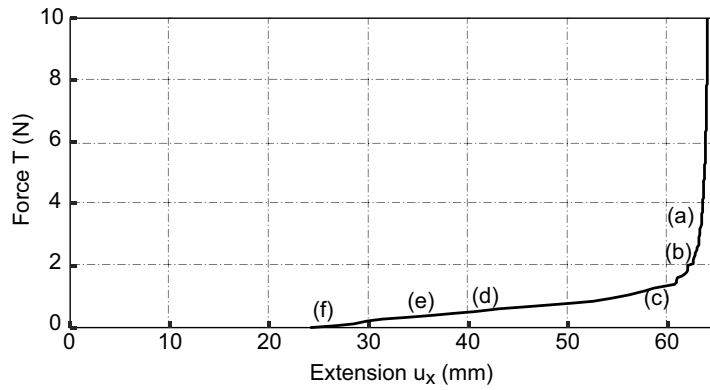


Figure 19: Simulation of uncoiling of a tape spring $r_c/R = 4.3$, along with snapshots of the simulated tape spring at points (a)-(f). Arrows indicate locations of localized folds, where the tape spring is more than 3x its thickness away from the hub.

the initial configuration for the coiling simulation in Section 5.1, where only two localized folds were present at $T = 0$. This result shows that the coiling/uncoiling process is path dependent.

Similar uncoiling simulations were performed for coiling ratios between 3 and 20. The results are summarized in a contour plot, Fig. 20, that shows the number of localized folds for different values of the coiling ratio, r_c/R , and the applied tension force. Note that the force required to avoid the formation of the first localized fold increases linearly with the coiling ratio and, for a chosen coiling ratio, the number of localized folds for $T \rightarrow 0$ also increases.

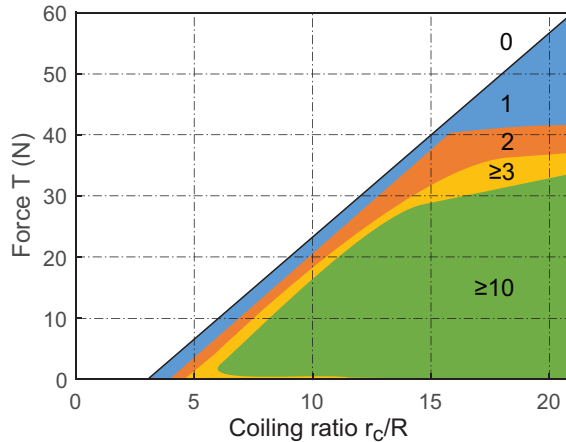


Figure 20: Number of localized folds during uncoiling of a tape spring as a function of tension force and coiling ratio.

Focusing specifically on the force required to maintain a smoothly coiled tape spring, Fig. 21 shows plots of the force limits obtained with three different ways of estimating the appearance of the first localized fold. These results were all obtained for uncoiling from an initial tension of 60 N. In Fig. 21(a) the cut off was computed with the tape spring midline method, and using either $\gamma = 305^\circ$ or $\gamma = 315^\circ$ for the angle over which the tape spring has to conform to the coiling cylinder. In Fig. 21(b) the spike in the force-extension derivative method was used. Note that both ways of estimating the cut-off lead to results

435 that follow a linear trend.

The coiling ratio range $r_c/R < 3.424$ was also investigated. In particular, for $r_c/R < 1$, the results provided by the simulations were in good agreement with the theoretical model developed in Section 2.1. In the range $1 < r_c/R < 3.424$, it was not possible to identify a clear trend in the tension force values obtained
440 from the simulations, as already seen in Fig. 18. The formation of localized folds and the existence of multiple competing deformation modes (with different numbers of folds) is responsible for the lack of a definite trend in this coiling ratio range.

6. Discussion and Conclusion

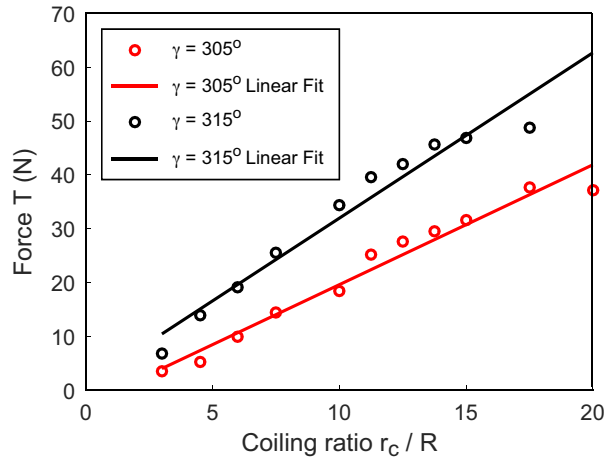
445 The opposite-sense coiling of tape springs around cylinders of different radii has been studied. One end of the tape spring was clamped to the cylinder and a tension force was applied at the tip end, to hold the tape spring coiled. The question, what is the smallest tension force required for the tape spring to conform to the cylinder, has been answered.

450 A key parameter is the coiling ratio, r_c/R , i.e. the ratio between the radius of the coiling cylinder and the natural radius of folding of the tape spring, which is equal to the cross-sectional radius of curvature, in the case of isotropic tape springs with uniform transverse curvature. A wide range of coiling ratios has been considered, through a combination of analytical studies, experiments and
455 detailed finite element simulations. Three different coiling regimes have been identified bending dominated, tension dominated, and an intermediate behavior between the two main regimes.

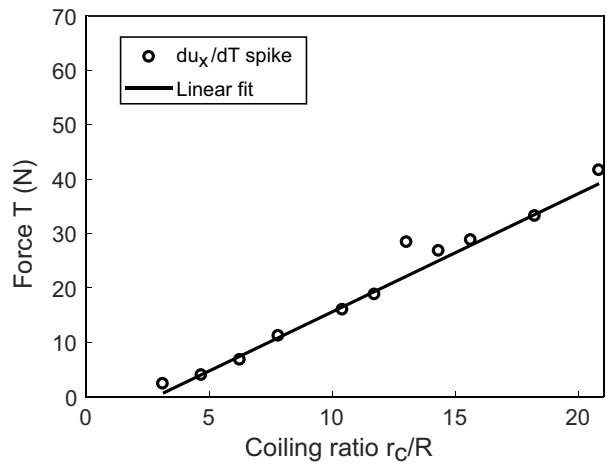
Bending-dominated behavior occurs for $r_c/R \leq 1$ and leads to an inverse quadratic relation between the tension and the coiling ratio. From Eq. 9:

$$T \propto \left(\frac{R}{r_c}\right)^2 - 1 \quad (20)$$

460 In this regime the tape spring tends to form a uniform coil, and the coiling and uncoiling behaviors coincide.



(a)



(b)

Figure 21: Tension force required to maintain a fully coiled tape spring using the midline approach method (a) and the spike in the derivative method (b).

Tension-dominated behavior occurs for $r_c/R > 3.424$ and leads to a linear relationship between tension and coiling ratio:

$$T \propto \frac{r_c}{R} \quad (21)$$

The tension force needed for the tape spring to conform to the coiling cylinder increases linearly with r_c/R and becomes infinitely large as $r_c/R \rightarrow \infty$. In this tension-dominated behavior, the constant of proportionality depends on how tightly the tape spring is required to conform to the coiling cylinder.

For intermediate coiling ratios, $1 < r_c/R < 3.424$ the bending-dominated analytical model, Eq 20, predicts compressive instead of tensile forces, but in reality in this range the coiled tape springs become unstable and small tensile forces have to be applied to hold them coiled.

The minimum tension force required to maintain a fully coiled tape spring is important for deployable structures applications. However, it is also interesting to understand how the number of localized folds relates to the tension force at lower force levels. The uncoiling simulations in Section 5.2 were used to generate Fig. 20, which shows the number of localized folds present during uncoiling, as a function of coiling ratio and tension force. The first fold consistently forms near the point of separation between the tape spring and the cylinder. As the force is decreased, a second localized fold forms, either adjacent to the first localized fold, or, as observed in Fig. 15, adjacent to the pinned end of the tape spring. As the force continues to decrease, localized folds rapidly form along the entire length of the tape spring. At very low tension forces the number of localized folds actually starts to decrease, as the folds grow large enough to merge. However, the larger the coiling ratio, the more localized folds will remain when the applied force is reduced to zero.

The finite element simulations of the coiling process are in good agreement with the experimental results that have been presented. They accurately predict the sequence of localized folds with increasing tape spring extension and the force profile as a function of the extension. Table 2 shows an overview of experimental observations and model predictions for the wrapping of a tape spring

with $r_c/R = 4.3$. Similar drops in force were observed after each bifurcation in both experiments and simulations, Fig. 22.

Localized Folds	Extension u_x (mm)		Force (N)	
	Experiment	Simulation	Experiment	Simulation
3	29.5	27.5	2.4	2.86
4	50.5	51.4	5.1	5.37
5	56.5	54.8	5.96	5.6
6	59.25	59.48	5.58	5.87

Table 2: Comparison of force immediately prior to bifurcation to a given number of localized folds, and corresponding extension, from experiment and simulation for tape spring with $r_c/R = 4.3$.

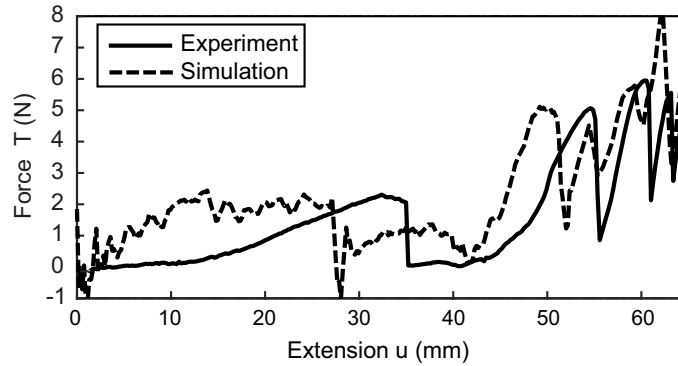


Figure 22: Comparison of force vs. extension for coiling experiment and simulation.

It is also noted that independent studies of coiling and uncoiling for large coiling ratios (tension-dominated regime) have given consistent results, both in
495 terms of the force magnitudes and for the linear variation of the tension force
required to maintain the tape spring conformed to the coiling cylinder. For
example, the minimum force predicted by an uncoiling simulation for $r_c/R = 5$
was 5.5 N, which is within the range of 4-15 N predicted by coiling simulations
that targeted different degrees of conformity of the tape spring to the coiling
500 cylinder.

Lastly, it is noted that the tension force required to hold a tape spring coiled is independent of the length of the tape spring, for lengths on the order of one coiled circumference or greater.

Acknowledgements

505 The authors are grateful to Antonio Pedivellano (Caltech) for helpful discussions. Financial support from the Northrop Grumman Corporation and the Space Solar Power Project at the California Institute of Technology is gratefully acknowledged.

Appendix - Details of finite element model

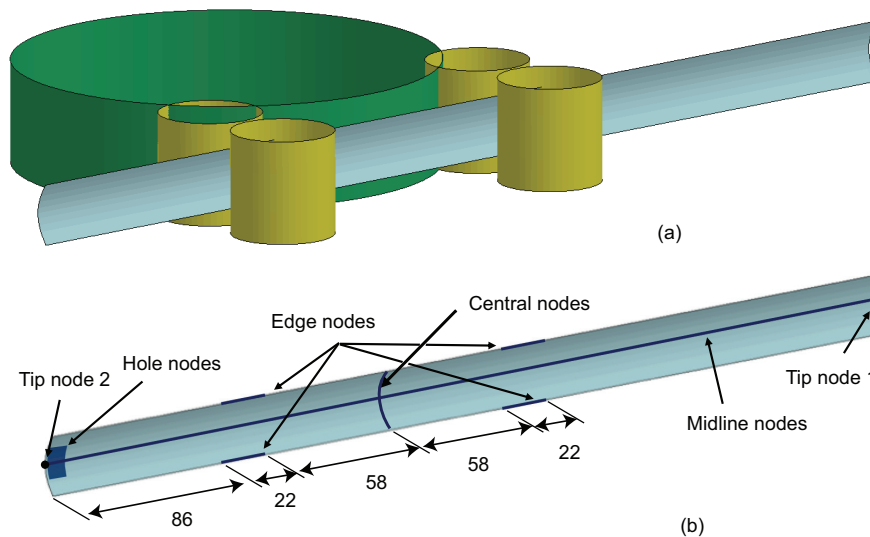


Figure 23: (a) Initial setup of tape spring coiling simulations in Section 4.1; (b) associated dimensions (in mm) and node sets.

510 The mesh sensitivity of the wrapping and unwrapping simulations was investigated by comparing the force-extension results between four meshes with different element edge lengths: 3 mm, 2.5 mm, 2 mm, and 1.5 mm. The results

Description	Time (s)	Node Set	Boundary Conditions Activated
Restrain out of plane displacement	0 - 0.17	Midline Nodes	$u_z = 0$
Restrain out of plane displacement	0 - ∞	Top end node	$u_z = 0$
Restrain out of plane displacement	0 - ∞	Bottom end node	$u_z = 0$
Edges are displaced to flatten tape-spring	0 - 0.04	Edge nodes	$u_x = 3.7 \text{ mm}$
Fix midline position as edges are flattened	0 - 0.06	Midline nodes	$u_x = u_y = 0$
Contact applied between tape spring and cylinders	0.04 - 0.16	All nodes	
Fix central nodes in Y	0 - 0.20	Central nodes	$u_y = 0$
Fix central nodes in X	0.16 - 0.20	Central nodes	$u_x = 0$
+Z end node displaced to fold tape spring around cylinders	0.06 - 0.21	Top end node	$u_x = f_1(t), u_y = g_1(t)$
-Z end node displaced to fold tape spring around cylinders	0.06 - 0.21	Bottom end node	$u_x = f_2(t), u_y = g_2(t)$
Damping applied to remove kinetic energy	0.17 - 0.21	All nodes	$\beta = 100 \text{ s}^{-1}$
Fix whole region	0.2 - ∞	All nodes	$u_x = u_y = 0$
End node held in place	0.20 - 0.21	End node	$u_x = u_y = 0$
Damping applied to reduce kinetic energy	0.21 - ∞	All nodes	$\beta = 1 \text{ s}^{-1}$

Table 3: Summary of simulation steps for wrapping an isotropic tape spring around a cylinder, where $r_c > R$. For the simulation results in Fig. 17, β was increased to 100 s^{-1} at $u_x = 53 \text{ mm}$ to reduce the build up of kinetic energy and correctly capture the bifurcation from four to five localized folds.

of the mesh sensitivity analysis are shown in Figs 24-25 for the wrapping and unwrapping simulations, respectively.

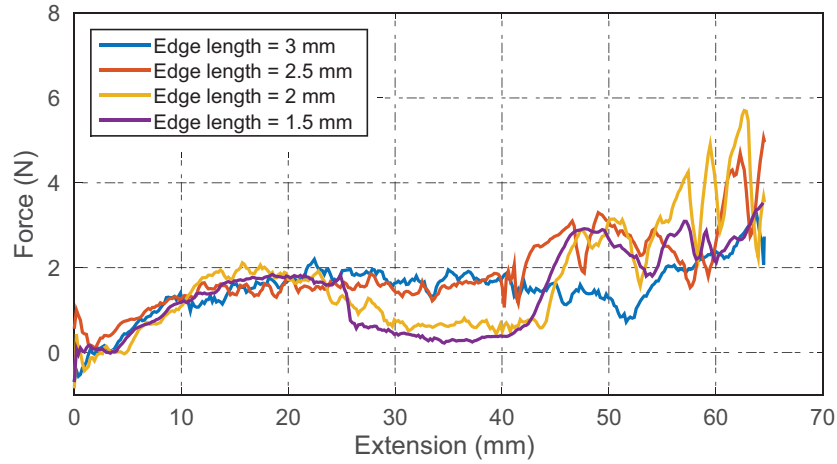


Figure 24: Force-extension for coiling of tape springs meshed with triangular C^0 shell elements with side lengths of 3 mm, 2.5 mm, 2 mm, and 1.5 mm. Mass nodal damping was set to $\beta = 10 \text{ s}^{-1}$, and the data was smoothed with a 5 point moving average to remove noise.

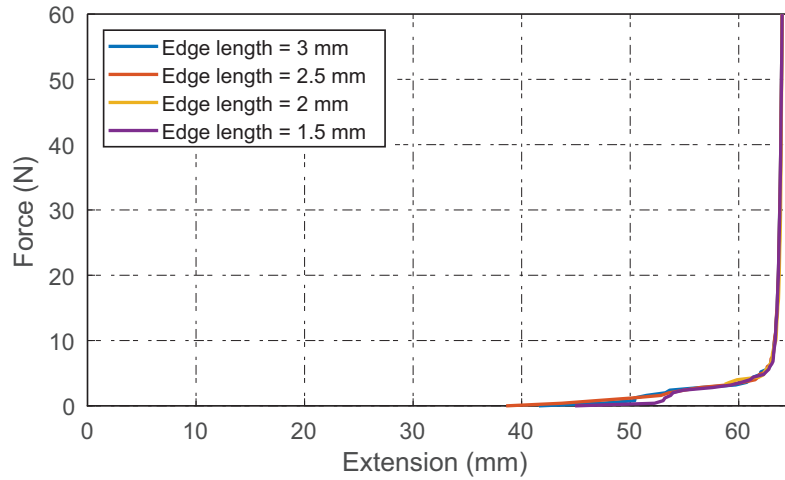


Figure 25: Force-extension for uncoiling of tape springs with $r_c/R = 6.25$ meshed with fully integrated quadrilateral shell elements with side lengths of 3 mm, 2.5 mm, 2 mm, and 1.5 mm.

515 **References**

- Arenberg, J., Flynn, J., Cohen, A., Lynch, R., Cooper, J., 2016. Status of the JWST sunshield and spacecraft, in: SPIE Astronomical Telescopes+ Instrumentation, International Society for Optics and Photonics, pp. 990405–990405.
- 520 Calladine, C.R., 1988. The theory of thin shell structures 1888–1988, Proceedings of the Institution of Mechanical Engineers, Part A: Journal of Power and Energy, 202 (3), 141–149.
- Calladine, C.R. and Seffen, K.A., 2019. Personal Communication.
- Dailey, D., Gilman, L., Parker, A., 1999. Precision deployable boom assembly,
525 US Patent 5857648A.
- Fang, H., Lou, M., Hah, J., 2006. Deployment study of a self-rigidizable inflatable boom, Journal of Spacecraft and Rockets 43 (1), 25–30.
- Guest, S. D. and S. Pellegrino, 2006. Analytical models for bistable cylindrical shells. Proceedings of the Royal Society A 462(3): 839-854.
- 530 Hallquist, J.O., 2007. LS-DYNA keyword users manual, Livermore Software Technology Corporation, 970th Edition.
- Hoskin, A., Viquerat, A., Aglietti, G.S., 2017. Tip force during blossoming of coiled deployable booms, International Journal of Solids and Structures, 118-119, 58 - 69, doi.org/10.1016/j.ijsolstr.2017.04.023.
- 535 Jeon, S., Murphey, T., 2011. Design and analysis of a meter-class cubesat boom with a motor-less deployment by bi-stable tape springs, 52nd AIAA/ASME/ASCE/AHS/ASC Structures, Structural Dynamics and Materials Conference, AIAA-2011-1731.
- Lappas, V., Adeli, N., Visagie, L., Fernandez, J., Theodorou, T., Steyn, W.,
540 Perren, M., 2011. Cubesail: A low cost cubesat based solar sail demonstration mission, Advances in Space Research 48 (11), 1890–1901.

- Leclerc, C., Wilson, L., Bessa, M., Pellegrino, S., 2017. Characterization of ultra-thin composite triangular rollable and collapsible booms. SciTech 2017. Grapevine (TX), AIAA-2017-0172, DOI 10.2514/6.2017-0172.
- 545 Mallol Parera, P., 2013. Deployment simulations of a composite boom for small satellites, Ph.D. thesis, KTH Royal Institute of Technology.
- Mauch, H. R., 1969. Deployable lattice column, US patent 3486279A.
- Murphey, T. W., Turse, D. E., Adams, L. G., 2017. TRAC boom structural mechanics. 4th AIAA Spacecraft Structures Conference, 9 - 13 January 2017, 550 Grapevine, TX, AIAA 2017-0171.
- Pellegrino, S., 2005. Bistable shell structures. 46th AIAA/ASME/ASCE/AHS/ASC Structures, Structural Dynamics and Materials Conference, 18-21 April 2005, Austin, TX, AIAA 2005-1934.
- Pellegrino, S. (2015). Folding and deployment of thin shell structures. In: Extremely Deformable Structures, edited by D. Bigoni, Springer: 179–267. 555
- Prentis, J.M., 1979. Engineering Mechanics. Oxford University Press.
- Schenk, M., Viquerat, A. D., Seffen, K. A., Guest, S. D., 2014. Review of inflatable booms for deployable space structures: packing and rigidization, Journal of Spacecraft and Rockets 51 (3), 762–778.
- 560 Seffen, K., Pellegrino, S., 1999. Deployment dynamics of tape springs, in: Proceedings of the Royal Society of London A: Mathematical, Physical and Engineering Sciences, 455, 1003–1048.
- Stabile, A., Laurenzi, S., 2014. Coiling dynamic analysis of thin-walled composite deployable boom, Composite Structures, 113, 429–436.
- 565 Straubel, M., Block, J., Sinapius, M., Huhne, C., 2011. Deployable composite booms for various gossamer space structures, 52nd AIAA/ASME/ASCE/AHS/ASC Structures, Structural Dynamics and Materials Conference, AIAA 2011-2023.

570 Straubel, M., Seefeldt, P., Spietz, P., Huhne, C., 2015. The design and test of the
GOSSAMER-1 Boom deployment mechanisms engineering model, 2nd AIAA
Spacecraft Structures Conference, AIAA 2015-1837, DOI: 10.2514/6.2015-
1837.

Wilson, L.L., 2017. Analysis of packaging and deployment of ultralight space
structures, Ph.D. thesis, California Institute of Technology.